ASME Journal of Mechanisms and Robotics
Online journal at:
https://asmedigitalcollection.asme.org/mechanismsrobotics

Vaughn Chambers[2]
Department of Mechanical Engineering,
University of Delaware,
Newark, DE 19716
e-mail: vaughn@udel.edu

Bradley Hobbs[2]
Department of Mechanical Engineering,
University of Delaware,
Newark, DE 19716
e-mail: bwh@udel.edu

William Gaither
Department of Mechanical Engineering,
University of Delaware,
Newark, DE 19716
e-mail: wgaither@udel.edu

Zachary Thé
Department of Mechanical Engineering,
University of Delaware,
Newark, DE 19716
e-mail: thezach@udel.edu

Anthony Zhou
Department of Mechanical Engineering,
University of California,
Berkeley, CA 94720
e-mail: anthonyzhou@berkeley.edu

Chrysostomos Karakasis
Department of Mechanical Engineering,
University of Delaware,
Newark, DE 19716
e-mail: chryskar@udel.edu

Panagiotis Artemiadis[1]
Human-Oriented Robotics and Control Lab,
Department of Mechanical Engineering,
University of Delaware,
Newark, DE 19716
e-mail: partem@udel.edu

The Variable Stiffness Treadmill 2: Development and Validation of a Unique Tool to Investigate Locomotion on Compliant Terrains

Understanding legged locomotion in various environments is valuable for many fields, including robotics, biomechanics, rehabilitation, and motor control. Specifically, investigating legged locomotion in compliant terrains has recently been gaining interest for the robust control of legged robots over natural environments. At the same time, the importance of ground compliance has also been highlighted in poststroke gait rehabilitation. Currently, there are not many ways to investigate walking surfaces of varying stiffness. This article introduces the variable stiffness treadmill (VST) 2, an improvement of the first version of the VST, which was the first treadmill able to vary belt stiffness. In contrast to the VST 1, the device presented in this paper (VST 2) can reduce the stiffness of both belts independently, by generating vertical deflection instead of angular, while increasing the walking surface area from $0.20\,m^2$ to $0.74\,m^2$. In addition, both treadmill belts are now driven independently, while high-spatial-resolution force sensors under each belt allow for measurement of ground reaction forces and center of pressure. Through validation experiments, the VST 2 displays high accuracy and precision. The VST 2 has a stiffness range of $13\,kN/m$ to $1.5\,MN/m$, error of less than 1%, and standard deviations of less than $2.2\,kN/m$, demonstrating its ability to simulate low-stiffness environments reliably. The VST 2 constitutes a drastic improvement of the VST platform, a one-of-its-kind system that can improve our understanding of human and robotic gait while creating new avenues of research on biped locomotion, athletic training, and rehabilitation of gait after injury or disease. [DOI: 10.1115/1.4066173]

Keywords: variable stiffness, gait, biped locomotion, rehabilitation, mechanisms and robots

1 Introduction

Legged locomotion, particularly human-like gait, is tremendously complex, especially when considering the variety of environments encountered on a daily basis. Each environment possesses distinct properties such as stiffness, damping, friction coefficient, slope, and roughness, necessitating a unique response to maintain stability and minimize energy expenditure [1]. This response has been shown to be highly dependent on robust coordination between the legs [2,3]. Of these surface properties, walking on low-stiffness environments has recently drawn much interest [4–6], as it has shown to be valuable for both human rehabilitation or training and the development of robust controllers for biped and quadruped robots. To further this area of study, there is a need for equipment that can repeatably and accurately simulate various walking environments with different properties.

There is much evidence to suggest that low ground stiffness walking is beneficial for understanding and rehabilitating human gait [7]. Gait dysfunction is a very common issue, especially

[1]Corresponding author.
[2]Both authors contributed equally to the manuscript.

Contributed by the Mechanisms and Robotics Committee of ASME for publication in the JOURNAL OF MECHANISMS AND ROBOTICS. Manuscript received December 24, 2023; final manuscript received July 30, 2024; published online September 3, 2024. Assoc. Editor: Joo H. Kim.

among those who have had a stroke [7–9]. The significance of implementing these ground stiffness perturbations, especially with respect to stroke rehabilitation, is in the disturbance of multiple neural pathways and, therefore, numerous brain areas. This disturbance can assist in relearning motor patterns through the concept of neuroplasticity [10–12]. Additionally, low ground stiffness walking may be beneficial to athletes, especially runners, when attempting to prevent overuse injuries or return to activity after an injury, by offering a low-impact environment to train [13,14]. In this case, a low-stiffness environment allows for reduced hip and knee forces resulting from heel strike, as well as creating a challenging walking environment to promote the muscular adaptations necessary for recovery [15–17].

Initial research in this area investigated the merit of reduced stiffness environments through walking overground on a variety of different surfaces. Many of these studies have examined how leg stiffness increases to maintain stability on low-stiffness terrain while walking [18], running [19], hopping [20], and with particular interest in the transition from rigid to compliant surfaces [19,21], as opposed to steady-state walking on the soft ground. Being able to correctly identify the differences in walking on rigid versus compliant ground has also been investigated with respect to stability measures [22], kinematics [23] and muscle activity [24,25]. Additionally, understanding energetic cost and biomechanics when running on soft surfaces has been examined [26]. In all of these studies, testing was limited to three or fewer different low-stiffness environments due to restrictions of using a collection of different materials to walk on or creating a spring-based platform, not allowing for an easy change of stiffness.

Low-stiffness environments are also incredibly useful for the development of robust controllers for biped and quadruped robots. As robots are used for a variety of applications such as industrial inspection, search and rescue, payload delivery, security, mining, and agriculture, having the ability to generate stable locomotion in most real-world environments is crucial [27]. With terrains of sand, mud, snow, and grass all having different mechanical stiffnesses, legged robots aim to be robust in environments ranging from rigid to rather compliant [28]. Multiple studies have investigated biped or quadruped robots walking on soft gym mats and other soft materials [6,29]. In a few studies, the quadruped or biped robot walks on multiple different low-stiffness environments by estimating compliance with onboard sensors in real time [29,30]. While most of these studies were conducted on less than three different surfaces, for the continued growth of this field, a more convenient and reliable way of testing a multitude of terrains is required. The ideal test environment would lend the ability to control ground stiffness in a laboratory setting, where devices such as motion capture cameras, electrodes, and force mats could still be easily used.

For the reasons discussed earlier, the variable stiffness treadmill (VST) 1 was previously created in our lab. The VST 1 was the first treadmill capable of altering vertical ground stiffness [31,32]. This treadmill is split-belt, where the speed of the belts is tied, but the stiffness of the belts is not. The VST 1 has the capability to reduce the stiffness of the left belt while keeping the right one rigid. Variable stiffness was achieved using a first-class lever system, where the two opposing forces were the subject's weight on the treadmill and the force of two extension springs in parallel. The effective stiffness (the stiffness felt by the subject) was able to be altered by changing the moment arm of the force applied from the walker (i.e., altering the mechanical advantage). By changing this distance via a linear actuator, stiffness levels ranging from 61.7 N/m to 1 MN/m were achievable on the left belt. It should be noted that the deflection created on this treadmill was angular, not linear. As the treadmill belt deflects, it rotates around a fulcrum at the front of the treadmill. Therefore, to create a constant effective stiffness underneath the walker's foot throughout a gait cycle, the linear actuator that controls the mechanical advantage between the belt and the springs had to constantly change its position as a function of the subject's foot position on the belt. While this is satisfactory, it is not ideal. This introduces a slight delay between the linear actuator position and the subject's foot position. Additionally, the angular deflection generated by the VST 1 causes the ankle to either increase dorsiflexion for the entire bottom of the foot to remain in contact with the belt or allow the heel to lift off the belt earlier in the stance phase. In either case, this angular deflection is not commonly seen in natural environments, and a treadmill with vertical deflection is more desirable.

Despite limitations, the VST 1 has been used to investigate human gait in various ways. First, the asymmetric environment created by the VST 1 has been shown to disrupt inter-leg coordination and generate responses to these low-stiffness perturbations [33–35]. In these studies, mainly right-side responses are seen in the ensuing gait cycles by perturbing the left leg via low-stiffness perturbations. Indications of an evoked inter-leg coordination response have been further validated via brain activity through both response delays and the use of electroencephalography [4,36]. Additionally, rehabilitation protocols directed toward post-stroke populations have begun to be tested on the VST 1 [5,37]. Specifically, it has been shown that walking in an asymmetric low-stiffness environment leads to aftereffects that could be useful for poststroke gait rehabilitation.

It should be noted that a device similar to the VST 1, the Treadmill with Adjustable Stiffness (TwAS), was recently designed and assembled by another research group [38]. This device had multiple improvements over the VST 1, such as vertical deflection (as opposed to angular) and variable stiffness control of both belts. However, this device has many drawbacks. First, the TwAS suffers from a lack of a counterweight to offload the weight of the belt. This causes an initial displacement of the belts at low stiffnesses before any external load is applied. This device does not allow for stiffness to be changed independently of deflection, which is undesirable in most circumstances. Additionally, the TwAS has a small walking surface with respect to length of only 0.98 m. With average step lengths of 0.79 m and 0.66 m for men and women, respectively, this does not give subjects, especially taller ones, enough space to walk comfortably [39,40]. Also, the device has a large distance between belts, which can cause unnatural foot placement, significantly affecting gait. Next, the TwAS lacks force sensors, which does not allow for center of pressure (CoP) tracking with human subjects. The lack of force sensors also does not allow for effective stiffness calculations over time as a subject walks, making it difficult to verify the magnitude of belt stiffness in dynamic scenarios [38,41]. Finally, and possibly most importantly, the TwAS has not been extensively tested and studied. To our knowledge, since it was designed in 2018, only a few experiments have been conducted to validate the device and the responses it creates, and no further peer-reviewed papers have been published.

Introduced in this article is the second iteration of the VST, the VST 2. The limitations of the VST 1 were the motivation for this device; therefore, many improvements have been made compared to the first iteration. First, to increase subject comfort when walking on the treadmill, the surface of each belt has been increased from 104 cm by 19 cm to 165 cm by 45 cm, and the treadmill height from the ground has been reduced from 74 cm to 45 cm. Those size improvements are very significant when it comes to human subject experiments as they allow not only improved safety and subject comfort, but higher walking speeds and even running speeds that were not feasible with the previous devices [31,32,38]. Next, the variable stiffness mechanism (VSM) creates a vertical deflection instead of an angular deflection. This is desirable as this will not force the ankle into more dorsiflexion and is more closely related to surfaces found in real-world settings. Additionally, and possibly most noteworthy, since the VST 2 deflects vertically, a constant effective stiffness can be created throughout the entire gait cycle without needing to update the VSM motor position. This gives a higher degree of accuracy and precision for the effective stiffness of the treadmill platform. Also, the VST 2 is capable of altering the stiffness of both belts independently, creating more possibilities

Fig. 1 The VST 2 with a subject walking on it while wearing a harness-based body weight support. The subject is equipped with 22 motion capture markers as well as 10 EMG electrodes tracking muscle activity. The left figure shows the right belt at a lower stiffness than the left, resulting in a vertical deflection. The right figure shows the opposite.

for environments that could be simulated. Next, the belts are controlled by separate motors, giving the capability of walking with the belts at different speeds, a feature that has been utilized in previous studies related to poststroke rehabilitation [42–44]. Finally, the VST 2 is equipped with high-resolution force sensors under both belts, allowing for the acquisition of center of pressure data for each foot, the total center of pressure path (butterfly diagram) [45], and resultant ground reaction force through estimation using the vertical force component. In the following sections, we describe the system in detail and present results showing the vertical stiffness controlled with less than 1% error across a wide range of stiffness values. In summary, the VST 2 is a significant improvement of a one-of-a-kind device, the VST 1, that allows a plethora of new studies and experimental protocols not possible before. Specifically, the VST 2 can be used to enhance our understanding of the mechanisms of human gait, create robust gait rehabilitation protocols, and aid in the design of controllers for legged robots, among others.

2 Device Design

The VST 2 combines multiple discrete subsystems into one complex device. Important subsystems that comprise the VST 2 include the VSM, dynamic split-belt treadmill platforms, drivetrain, electrical and control system, counterweights, force mats, and body weight support (BWS). The full system is depicted in Fig. 1, and the specifications of each of these subsystems are discussed below.

2.1 Design Specifications. The first set of specifications involves the variable stiffness capabilities of the VST 2 and revolves around high-level features, as well as stiffness and motion ranges. In order to have the ability to apply stiffness perturbations to either leg, the VST 2 is designed to be bilaterally compliant with independently adjustable stiffness levels for each belt. The VST 1 was only capable of varying the stiffness of the left belt, while the right belt would always remain rigid. The upgrade to bilateral compliance expands gait research possibilities and allows for testing a host of new hypotheses. The selection of a 1 MN/m–10 kN/m stiffness range allows for simulating a variety of surfaces from effectively rigid at 1 MN/m to highly compliant at 10 kN/m [46], and aligns with the previous research in this area. In order to more closely match real-world environments as well as improve upon the design of the VST 1, the deflection of the loaded treadmill platforms is designed to be vertical as opposed to angular. Specifically, the system allows for 10 cm of maximum linear travel, allowing for the capacity to handle 1 kN of force at a stiffness of 10 kN/m. The 0.07 N/m average stiffness adjustment resolution and 400 ms travel time between rigid and minimum stiffness permit precise and rapid stiffness changes. A counterweight system (CWS) is included, ensuring only VSM forces are transmitted to the subject and ensuring constant static deflection when set to low stiffness in the absence of external forces.

The second set of specifications pertains to the split-belt treadmill component of the VST 2, specifically with treadmill performance, safety, and comfort. To accommodate the range of normal walking speeds, the treadmill component is designed for a speed range of −2.6 m/s to 2.6 m/s on each belt, with positive and negative speed denoting the ability of the treadmill belts to move in both directions. Additionally, as split-belt treadmills are most commonly used for speed perturbations (i.e., belts moving at different speeds) [43,44,47,48], the VST 2 implements independent variable belt speed and a velocity resolution of 0.1 mm/s. To ensure subject safety and comfort, the treadmill platform height relative to the ground is 45 cm at the highest position. The treadmill belt width and the length minimally modify the gait of subjects and accommodate the stride length of tall individuals, with the belt width being 45 cm and the length being 165 cm. Additionally, the inter-belt distance is minimized to 15 mm. The fully assembled VST 2 platform

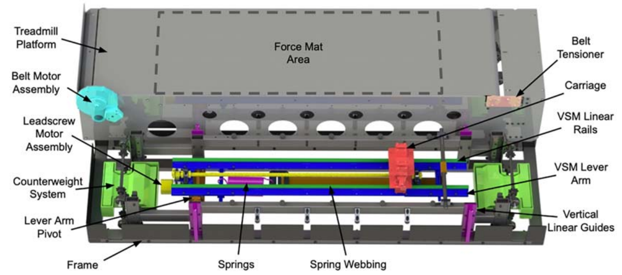

Fig. 2 The VST 2 with the right treadmill platform removed to expose inner mechanisms

is shown in Fig. 1. The VST 2 also features high-spatial-resolution force sensors beneath each belt to measure the ground reaction forces of both feet throughout the stance phase.

2.2 The Variable Stiffness Mechanism. At its core, the VSM is a third-class lever-based system that modifies the mechanical advantage between the platform and a set of fixed stiffness extension springs. This creates a variable effective stiffness at the platform that is dependent upon the geometric configuration of the system, contrasting other mechanisms that must be compact [49,50] or have more than one actuator [51–53], while being able to have simpler control design and able handle much higher working loads.

A color depiction of the VSM is shown in Fig. 2. The treadmill platform (light gray), constrained to move vertically by the vertical linear guides (purple) is supported by the carriage (red) via the linear rails on the bottom of the platform. The carriage serves as the movable connection point between the platform and the VSM assembly and rides on the VSM linear rails (green). Together, the carriage, VSM linear rails, and the leadscrew-motor assembly (yellow) form a linear actuator that allows the carriage to be positioned along the VSM lever arm (dark blue). The VSM lever arm pivots about the axle (orange) toward the rear of the treadmill. Toward the front of the treadmill, the end of the VSM lever arm is supported by the spring webbing (brown), which is fixed to the frame and wraps down and around a roller before coming parallel to the VSM lever arm. Under the VSM lever arm, the other end of the spring webbing connects to the extension springs (magenta), which are fixed to the bottom of the VSM lever arm. Thanks to the roller, any deflection of the VSM lever arm requires the extension of the spring webbing and a corresponding extension in the springs, generating a spring force that acts at the end of the VSM lever arm and resists the force applied to the platform.

This VSM design changes the effective stiffness by varying the mechanical advantage between the platform and the main springs through changes in the carriage position and, by extension, the point of platform force application to the VSM lever arm. Maximum effective stiffness is achieved when the carriage (red) is placed directly above the VSM lever arm pivot (orange). Note that Fig. 2 displays VSM at its minimum stiffness configuration. With the carriage in the maximum stiffness configuration, forces applied to the platform are transferred directly through the carriage, VSM axle, and into the frame of VST 2, resulting in the absence of platform deflection. As the carriage is moved away from the pivot and toward the end of the lever arm, the mechanical advantage

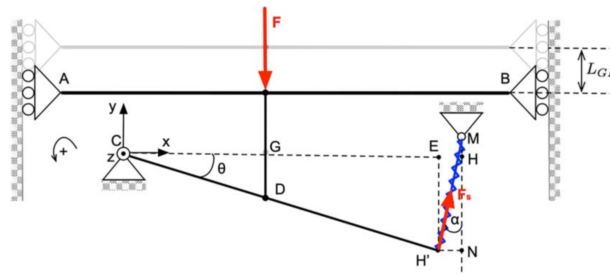

Fig. 4 The variable stiffness mechanism at an arbitrarily low stiffness, resulting in a deflection when force is applied

between the platform and the extension springs increases, resulting in a lower effective stiffness for carriage positions further from the pivot. The shown configuration of the VSM in Fig. 2 is at minimum stiffness with the highest mechanical advantage. For any carriage position other than the maximum stiffness case described earlier, a force applied to the platform results in a linear deflection of the platform, creating an angular deflection in the VSM and forcing the extension springs to elongate via the spring webbing. This generates a spring force that resists the force applied to the platform and results in an effective platform stiffness that is proportional to the carriage position and the spring coefficient of the extension springs.

The VST 2 simplified kinematic diagram is shown in Fig. 3(*a*). The VSM, along with the treadmill, is shown at equilibrium, where the spring is at its rest length. The mechanism can be simplified as shown in Fig. 3(*b*), where the equivalent spring is at its rest length and shown between points M and H. Figure 4 shows the deflection of the spring under a force **F** exerted on the treadmill, causing a vertical deflection of the treadmill by L_{GD}. Throughout this analysis, the notation L_{XY} will denote the scalar representing the Euclidean distance between the points X and Y. At this configuration, setting the sum of the torques around point C equal to zero gives:

$$\mathbf{F} \times \mathbf{CD} + \mathbf{F_s} \times \mathbf{CH'} = \mathbf{0} \tag{1}$$

where $\mathbf{F} = [0 \quad -F \quad 0]^T$ is the force exerted to the treadmill perpendicular to its surface pointing along the inertial reference axis y with magnitude $F > 0$, $\mathbf{CD} = [L_{CD}\cos(\theta) \quad -L_{CD}\sin(\theta) \quad 0]^T$ and $\mathbf{CH'} = [L_{CH'}\cos(\theta) \quad -L_{CH'}\sin(\theta) \quad 0]^T$ are the vectors **CD** and **CH′** expressed with respect to the inertial reference system at C, respectively, and $\theta > 0$, while $\mathbf{F_s} = \left[F_s\cos\left(\frac{\pi}{2} - \alpha\right) \quad F_s\sin\left(\frac{\pi}{2} - \alpha\right) \quad 0\right]^T = [F_s\sin(\alpha) \quad F_s\cos(\alpha) \quad 0]^T$ is the force exerted by the spring. Substituting these expressions in Eq. (1), the total torque along the z inertial axis are given by:

$$FL_{CD}\cos(\theta) - F_s L_{CH'}\cos(\alpha - \theta) = 0 \tag{2}$$

The force F_s exerted along the direction of the spring is given by:

$$F_s = k_s(L_{MH'} - L_{MH}) \tag{3}$$

where k_s is the stiffness of the spring, L_{MH} its rest length shown in Fig. 3(*b*), and $L_{MH'}$ is elongated length as shown in Fig. 4. From the diagram in Fig. 4, we have:

$$L_{MH'} = \frac{L_{MN}}{\cos(\alpha)} \tag{4}$$

where

$$L_{MN} = L_{MH} + L_{HN} = L_{MH} + L_{EH'} \Rightarrow$$
$$L_{MN} = L_{MH} + L_{CH'}\sin(\theta) \tag{5}$$

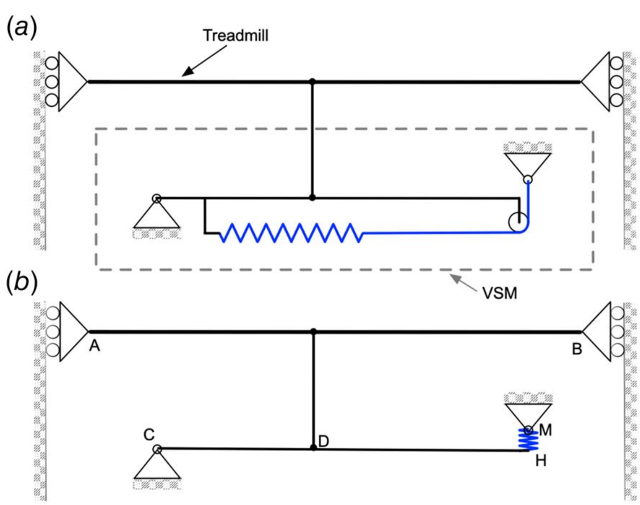

Fig. 3 Simplified kinematics of VST 2, where (*a*) shows the actual spring positioning and (*b*) shows an equivalent resting spring that will be used for the kinematic derivation

Then, from Eqs. (3)–(5), we have:

$$F_s = k_s\left(\frac{L_{MH} + L_{CH'}\sin(\theta) - \cos(\alpha)L_{MH}}{\cos(\alpha)}\right) \tag{6}$$

The total effective vertical stiffness of the treadmill k_e can be expressed as the ratio of the magnitude of the vertical force F exerted over the vertical displacement L_{GD} caused, i.e.,

$$k_e = \frac{F}{L_{GD}} \tag{7}$$

where $L_{GD} = L_{CD}\sin(\theta)$. By solving Eq. (2) for F, we have:

$$F = \frac{F_s L_{CH'}\cos(\alpha - \theta)}{L_{CD}\cos(\theta)} \tag{8}$$

From Eqs. (8) and (6), and since $L_{GD} = L_{CD}\sin(\theta)$, Eq. (7) is written as follows:

$$k_e = k_s\frac{L_{CH'}\cos(\alpha-\theta)(L_{MH}(1-\cos(\alpha)) + L_{CH'}\sin(\theta))}{L_{CD}^2\cos(\theta)\sin(\theta)\cos(\alpha)} \tag{9}$$

If we assume that the angle α is very small, i.e., $\alpha \simeq 0$, then $\cos(\alpha) \simeq 1$, and $\cos(\alpha - \theta) \simeq \cos(-\theta) = \cos(\theta)$, and therefore, Eq. (9) is simplified to:

$$k_e = k_s\frac{L_{CH'}^2}{L_{CD}^2} \tag{10}$$

Equation (10) shows that since $L_{CH'}$ is constant and given by design, controlling the effective vertical stiffness of the treadmill can be done by only controlling the distance L_{CD} from the fixed pivot point C to the carriage point D.

With a general system finalized and governing equations derived, the design space is explored in order to select specific components and dimensions for the system. As seen in Eq. (9), the true effective stiffness at the platform is a function of spring stiffness, lever arm length and the position of the carriage. With the length of the lever arm set, Eq. (10) is used to determine the spring stiffness needed to achieve the specified variable stiffness range of 1 MN/m to 10 kN/m. Based on this calculation, a bank of two 4.3 kN/m extension springs in parallel is implemented, yielding a theoretical minimum effective stiffness of 8.6 kN/m. The rest of the VSM accommodated the 1 m lever arm and the two 4.3 kN/m springs in parallel.

Highlighting a few of the main components, a 1 m long, 16 mm diameter leadscrew is chosen, which has an advancement of 35 mm per revolution. Additionally, the Teknic ClearPath CPM-SCHP-3446D-ELNA (Teknic Inc., Ontario County, New York) motor is chosen for control of the VSM. This motor has a peak power of 1531 W and a peak torque of 5.6 Nm, which is sufficient to reliably and quickly move the carriage to change stiffness levels.

2.3 Treadmill Platform Design. The treadmill portion of the design consists of the top portion of the carriage assembly that supports the external mass applied to the system, as well as the side panels to contain the frame-connected linear bearings, the belt-roller system, the drivetrain system, and the frame. The frame consists of 50 mm by 25 mm extruded low-carbon steel rectangular tubing of 2 mm thickness and is welded together as a single rigid body for the entire system (see Fig. 2). The frame houses multiple bolted interfaces to several other sub-assemblies in strategic positions, namely, the linear rails and the counterweight system. The frame also holds two rows of four gusset brackets that each house a single 30 kg-rated threaded rubber bumper of 40A durometer. The platform interfaces with these bumpers both in the event of reaching the maximal deflection of 10 cm and every time the platform returns to resting position from a deflection.

The CWS is required for the proper functioning of the VSM, with the purpose of ensuring the forces acting on the VSM are equal to zero when the treadmill is unloaded (see light green components in Fig. 2). The primary action required of the CWS is to travel in the opposite direction of the platform assembly during platform deflection and return when the platform reaches its neutral position. The CWS design is a chained system driven by a single-strand ANSI Number 40 roller chain, which is equal to the weight of the platform assembly and rests on the top half of the VSM carriage, with support from the frame. Four individual chain links contain rigid attachments that connect to a custom steel plate welded tray that holds custom-molded and painted lead weights of 34 kg each to precisely offset the 68 kg platform weight. This system is attached on both ends of each belt and is centered laterally relative to each belt, resulting in four counterweights in total. With the lever arm weight considered negligible in most configurations, the combination of two counterweights and one platform results in a total sprung system weight equal to 136 kg. This results in a large system inertia; however, since the nature of this device is to deflect under a range of forces consistent with average to above-average human weight during walking, the resulting accelerations are kept small, minimizing the affects of large inertia under normal experimental conditions. The overall vertical deflection of the platforms is measured by a 0.2 deg resolution, 12-bit absolute encoder (AMT222A-V, CUI Devices) at the CWS bearings, offering a direct relationship between CWS rotation and platform deflection.

The platform connects to the CWS through the side panels and has the primary function of connecting the belt and motor system, as well as interfacing with the CWS and linear rails. These panels are constructed from a 6.35 mm aluminum plate and contain circular screened cut-outs to reduce weight and allow for the viewing of the internal mechanisms of the VST 2. The outer face of the inner side panels for each side of the VST 2 contains only countersunk-head fasteners in order to attain a gap between treadmill belts of only 15 mm. The two side panels are rigidly connected through ten 20 mm solid t-slotted framing rails and through two ultra-strength high carbon steel cylinder belt rollers of 44.5 mm diameter and 2.5 mm wall thickness. The framing rails interface directly with the VSM through another set of VSM linear rails that are rigidly attached, allowing for a single connection point at the carriage at a 20 mm diameter 1566 carbon steel rotary shaft. The belt rollers interface directly with the belt and are doubly supported to each side panel through flanged ball bearings. The side panels also interface with the frame through four stainless steel linear guideway rail bearings at each corner of each side of the VST 2. These bearings constrain the deflection of the treadmill to a single degree-of-freedom acting as a vertically oriented prismatic joint, which ensures only vertical deflection and mitigates angular movement due to the VSM lever arm angular motion forces that are inherent in this system. This linear deflection is the most notable and substantial improvement from the previous version of this system (VST 1), which instead employs a revolute joint for only rotational deflection.

The front roller acts as a passive idler and includes a threaded tension mechanism for which to adjust the belt tension (see light-pink in Fig. 2). The rear roller acts as the treadmill belt driver and is connected with a 20 mm solid carbon steel keyed shaft to the treadmill drive motor (Teknic CPM-SCHP-3446D-ELNA; peak power: 1531 W; peak torque 5.6 Nm; Teknic Inc.) through a pulley reduction. The reduction consists of two zinc spoked v-belt

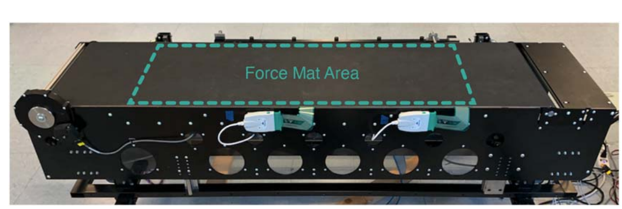

Fig. 5 One VST 2 platform with force mats installed

pulleys with pitch diameters of 6.35 cm and 24.77 cm, respectively, which transmit power through a Gates EPDM AX-24 v-belt and are completely enclosed by a custom plastic cover. Finally, the belts chosen are of custom length for this application and originate from a Precor C956i commercial treadmill (Precor). The walkable surface area for each belt is 0.74 m^2. Directly under each belt is a 20 mm thick particle board that supports the weight of the walker on the treadmill.

2.4 Additional Components. Under each of the treadmill belts are force sensor mats (Tekscan 3140 with VersaTek Cuffs, TekScan Inc., Norwood, MA) capable of acquiring vertical force measurements using 8448 individual capacitive sensing cells across both treadmill belts, offering a planar resolution of less than 1 cm in both directions (see Fig. 5). This gives the unique ability to observe both the distribution of forces from the foot and the foot center of pressure. These data are streamed live at a frequency of 65 Hz.

The custom-made harness-based BWS chosen (Litegait Inc., Tempe, AZ) for this application is fastened to the ground at the rear of the VST 2 and overhangs directly onto the center of the belts. This system has a maximum subject weight of 140 kg, and the amount of support can be adjusted for the specific application, while its height is adjustable through an actuator that moves the support vertically.

2.5 Control Architecture. For a given desired effective stiffness k_e^d, the corresponding desired VSM carriage position L_{CD}^d is determined via Eq. (10), represented by the function f_1 in Fig. 6(*a*). When the motor arrives at the desired position, the target carriage position L_{CD} is achieved, and the platform has a certain deflection according to the force applied and the effective stiffness. This displacement L_{GD} is measured by the deflection encoders integrated into the counterweight system which provide feedback on the platform displacement at a frequency of 200 Hz. The applied force F_f is measured at a rate of 100 Hz by the force sensing mats beneath each belt. The final effective stiffness k_e is a function of the kinematics and dynamics of the system and is dependent upon the applied force F_f and the platform deflection L_{GD}. This relationship is captured by the function f_2 in Fig. 6(*a*), which outputs the effective stiffness of the system for a given applied force and platform displacement. With respect to stiffness the system is open loop, with no feedback on the actual effective stiffness being used to optimize the performance of the system. This does open up the possibility for discrepancies between the true effective stiffness and the desired effective stiffness. However, since the effective stiffness is only a function of the carriage position, which is controlled through a closed-loop system, this error is mitigated by calibrating the VSM controller using experimental data, a process that is discussed in Sec. 3, along with the VSM performance evaluation.

The treadmill belts are controlled in a very similar way to the VSM, with the primary difference being that the treadmill belts utilize velocity control as opposed to position control (see Fig. 6(*b*)). When a new speed V^d is set in the control program, the needed angular velocity at the motor ω^d is calculated using the function f_3 and is sent to the motor drivers via USB connection. The motor drivers, which are running closed-loop velocity control on the belt motors at a loop frequency of 8 kHz, then drive the belt motors to the desired velocity using pulse-width modulation of 48 V and up to 100 A of current. As with the VSM motors, feedback is provided to the motor drivers by a 0.25 deg resolution, 8192 count incremental quadrature encoder (AMT102-V, CUI Devices) connected to each belt motor. The true belt speed V is a function of the system dynamics and the angular motor velocity ω, a relationship that is captured by the inverted function f_3^{-1} in Fig. 6(*b*). Unlike the VSM control system that has no feedback on the value of the true effective stiffness, the treadmill belt velocity is dependent upon only the angular motor velocity and thus is a fully closed-loop and accurate system.

3 System Evaluation and Results

The VST 2 was evaluated through two preliminary experiments. First, theoretical stiffness values from Eq. (10) were compared to stiffness values found experimentally. Second, the step response of the VST 2 was analyzed.

3.1 Stiffness Evaluation. The accuracy of the VSM of the VST 2 was first evaluated by comparing experimental results with the theoretical stiffness curve from Eq. (10). The discrepancy between the experimental and theoretical curves resulted in a new stiffness mapping that will replace Eq. (10) in the areas of "useful" stiffness ranges. The experimental procedure and results are explained in more detail below.

A known weight of 70 kg was used to evaluate the stiffness of a single treadmill platform with the VSM carriage at many different locations. Barbell plates, the weight of which was verified using a scale, were used for the 70 kg weight. This specific weight was chosen as it represents the average weight of all 12 subjects that partook in a recent study on the first version of the VST [5]. The VSM was tested at 13 different locations, taking the carriage across its full travel in increments of 5000 motor counts or 65 mm of linear travel. At each of the 13 locations, the 70 kg weight was applied to the center of the treadmill platform three times, and an average vertical deflection was taken between the three trials. Instead of physically dropping 70 kg of weight on the treadmill several times, the weight was simply left on the top of the treadmill for the entire experiment. The treadmill platform was manually lifted from the front and back until the rubber stoppers that limit its upward movement were fully engaged, ensuring that the VSM was fully unloaded and there was no vertical deflection. The front and back of the treadmill were then dropped simultaneously, allowing

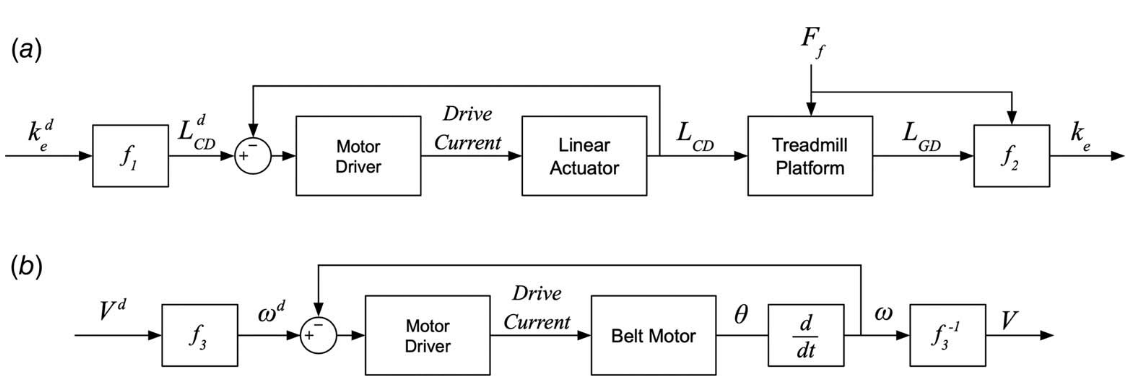

Fig. 6 Block diagrams for (*a*) the variable stiffness mechanism and (*b*) the treadmill belts

for the platform and weights to deflect and arrive at a new vertical position. The deflection was measured via an 8-camera Vicon motion capture system at 100 Hz (Vicon Motion Systems Ltd., Oxford, UK), which has a position error of less than 0.25 mm. Specifically, the 3D positions of three reflective markers, which were attached at the front, middle, and back of the platform, were recorded. For each trial, an average value was taken across the three markers to estimate the vertical position of the center of the treadmill. However, for all trials, the difference between front and back encoders was so small that the platform had a pitch angle of less than a tenth of a degree.

The resulting experimental stiffness curve is shown in Fig. 7. The difference between the experimental and theoretical stiffness values seems to be larger at high stiffness values, while decreasing as stiffness decreases. This could be due in part to the theoretical calculation not accounting for both friction and binding that can occur in a mechanism of this complexity. Additionally, high stiffnesses are far more sensitive to error and variation due to the corresponding very small deflection values. On this end, it should be noted that small variation is mostly required for lower stiffness values, where the effect of the treadmill stiffness is amplified. For instance, a 10 kN/m variation of treadmill stiffness around 60 kN/m would lead to a negligible 2 mm variation in deflection for the load in question, while a 10 kN/m variation of treadmill stiffness around 20 kN/m would lead to a significant 24 mm variation. While there is a significant discrepancy between experimental and theoretical curves, consistency of stiffness values, or small standard deviations, is far more important. This is due to the fact that the control architecture of the VST 2 will simply use a new mapping between carriage position and stiffness level to accurately simulate surfaces of a certain stiffness. It should also be noted that the seven data points corresponding to a carriage position of less than 500 mm were omitted from this analysis. For brevity, the authors decided to highlight only the "useful" stiffness range of 10–80 kN/m, which has been utilized extensively in the experiments of our group with VST 1 [4,5,24,25,33–37]. A carriage position of 78.75 mm was considered sufficiently rigid, as it was the first position where less than 0.1 mm treadmill deflection was measured during the weight loading (>6.8 MN/m). For this reason, the VSM carriage will not be used in configurations of less than 78.75 mm, reducing the overall travel of the carriage and decreasing the time it takes for the treadmill to switch between rigid to minimum stiffness from 467 ms to 400 ms.

Next, it should be noted how the device will be used in practice. Each belt of the VST 2 will always function in either one of two settings: "rigid" or "low-stiffness." For the "rigid" setting, the VSM will create a surface of high stiffness, simulating walking on a regular treadmill belt. In this case, a value of at least 6.8 MN/m was achieved with a carriage position of 78.75 mm. This stiffness is sufficiently high and much higher than the maximum stiffness achieved in the first iteration of the VST [32]. In the "low-stiffness" setting, the VSM will create a surface with a stiffness of less than 80 kN/m. When the stiffness value is higher than 80 kN/m the resulting deflections are so small, and therefore the VST 2 surface is indistinguishable from a rigid case described above. Therefore, stiffness levels between 6.8 MN/m and 80 kN/m will not be useful in human experiments and will not be discussed or explored any further.

Since the "rigid" case and the carriage position to achieve this stiffness have already been found, the region of "low-stiffness" values must be investigated. Figure 7 shows all experimental stiffness values less than 80 kN/m compared to theoretical stiffness values. The best-fit curve of the experimental data is also shown. As a reminder, this experiment was performed by setting a carriage position to measure stiffness at each position. However, in practice, the VST 2 will be used in the opposite configuration (i.e., a carriage position will be calculated based on a desired stiffness level). Therefore, a new mapping and a replacement to Eq. (10), as well as f_1 in Fig. 6(*a*), is found to be the inverse of the best-fit curve in Fig. 7 and can be described as follows:

$$L_{CD} = \begin{cases} a, \text{ if "rigid"} \\ b(k_e)^c + d, \text{ if "low } - \text{stiffness"} \end{cases} \tag{11}$$

where L_{CD} is the carriage position in *mm* as shown in Fig. 4, a is 78.75, b is 3188, c is –0.5804, d is 237.9, k_e is the effective vertical stiffness of the treadmill platform in kN/m, "rigid" is the maximum treadmill stiffness of at least 6.8 MN/m, and "low stiffness" represents the stiffness levels useful for human experiments, ranging from 18 to 80 kN/m. This fit has very little error with an R^2 value of 0.9998 and will allow for the generation of accurate low-stiffness surfaces.

3.2 Step-Response Analysis. Using the same protocol as described in Sec. 3.1, the treadmill platform deflection was tracked over time for six different stiffness levels. Stiffness levels of 21, 26, 33, 45, and 63 kN/m were evaluated as they span a typical range of stiffness levels used for experiments on the original VST. Additionally, a stiffness of 18 kN/m was also evaluated since it is the minimum stiffness level of the VST 2. It should be noted that for this analysis, the stiffness mapping shown in Eq. (11) was used and will be used for all future experiments and analyses.

As shown in Fig. 8, the deflection mimics an underdamped second-order system. The treadmill platform deflects, overshoots, and settles back to its desired steady-state value for each of the

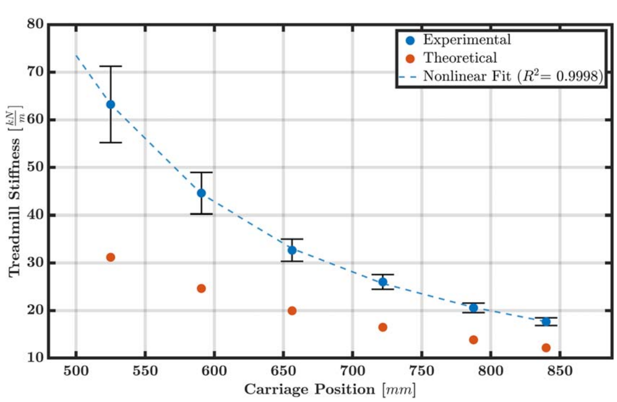

Fig. 7 Experimental stiffness values tested with 70 kg at six different values of the carriage position and compared to theoretical stiffness curve. Blue and orange points denote the average experimental and theoretical stiffness values, respectively, while black error bars indicate variations of one standard deviation across trials. The blue dashed line represents the best-fit curve of the experimental data.

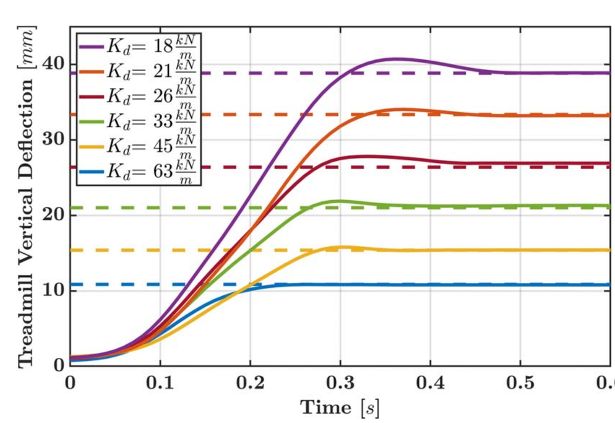

Fig. 8 Step responses with a 70 kg static mass at stiffness levels of 18, 21, 26, 33, 45, and 63 kN/m. Solid and dashed lines denote the actual and desired treadmill vertical displacement for each stiffness level, respectively.

six different stiffness levels. All six stiffness levels come to rest within 0.6 s, each approaching a distinct steady-state value with an error of less than 1.5%. Response specifications can be seen for each stiffness level in Table 1, where t_r is the rise time, t_s is the settling time, and e_{ss} is the steady-state error of these open-loop step responses.

To summarize, the validation of the VST 2 shows that it can simulate a wide range of stiffness values with both high accuracy and consistency. Low-stiffness values are accurate to within 1.5% and have a standard deviation of less than 10 kN/m. Future experiments with human subjects will further evaluate the VST 2. This will specifically focus on the human response to the perturbations generated on this device with respect to kinematic, muscle activity, and force mat data. We present a summary of the results of our experiments with a human subject below.

3.3 Human Data. A short human subject experiment was conducted to display preliminary results, mainly pertaining to the new capabilities of VST 2 compared to VST 1. The protocol for this study was approved by the University of Delaware Institutional Review Board (IRB ID: 1544521-2), with informed consent given by all subject participants. For this experiment, one able-bodied subject (height: 1.89 m, weight: 90 kg) walked on the treadmill in seven different configurations: rigid and unilaterally (right-side) compliant at 63 kN/m, 45 kN/m, 33 kN/m, 26 kN/m, 21 kN/m, and 18 kN/m. The subject walked at a speed of 1 m/s in each environment for approximately 60 s. For each of these scenarios, data were averaged over 50 gait cycles. These averaged data are the data discussed below. The motion of the subject and the treadmill platform were tracked using reflective markers and a motion capture system (Vicon Motion Systems Ltd.) with eight cameras around the treadmill capturing data at 100 Hz. The center of pressure path of the subject was tracked using the force mats (Tekscan 3140 with VersaTek Cuffs, TekScan Inc.) located under the treadmill belt capturing at 65 Hz. The center of pressure path was normalized using the subject's center of mass position,

Table 1 Open-loop response time specifications

K_d (kN/m)	t_r (s)	t_s (s)	e_{ss} (%)
18	0.1825	0.4509	0.0569
21	0.1843	0.4279	0.4487
26	0.1668	0.4088	0.4559
33	0.1642	0.3370	1.3646
45	0.1656	0.3333	0.2335
63	0.1284	0.2306	0.4697

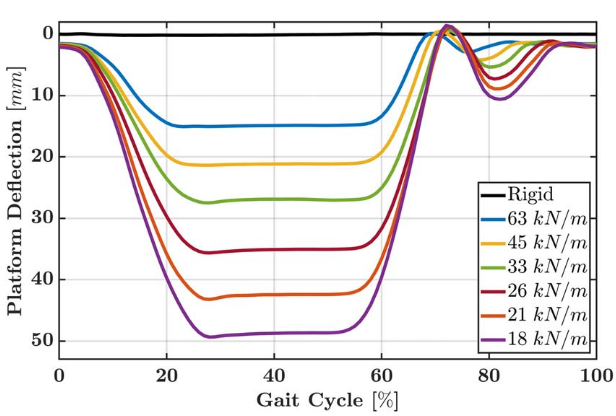

Fig. 9 Deflection of the platform over a single gait cycle at multiple stiffness levels with a 90 kg subject. A position of 0 mm corresponds to the unloaded, rigid platform. Note: The low-stiffness perturbations were unilateral. 0% at the gait cycle denotes the heel-strike event.

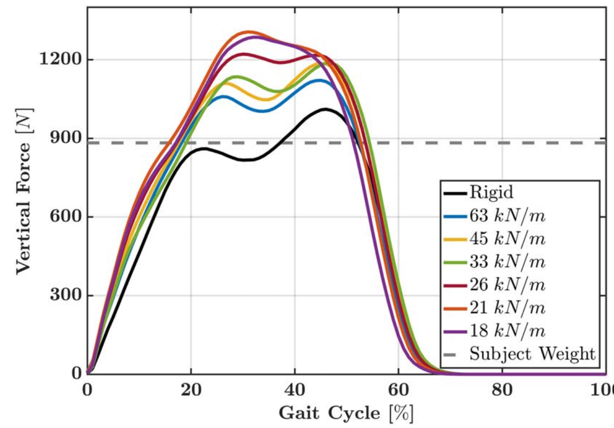

Fig. 10 Force applied on a single platform over a gait cycle at multiple stiffness levels with a 90 kg subject. 0% at the gait cycle denotes the heel-strike event.

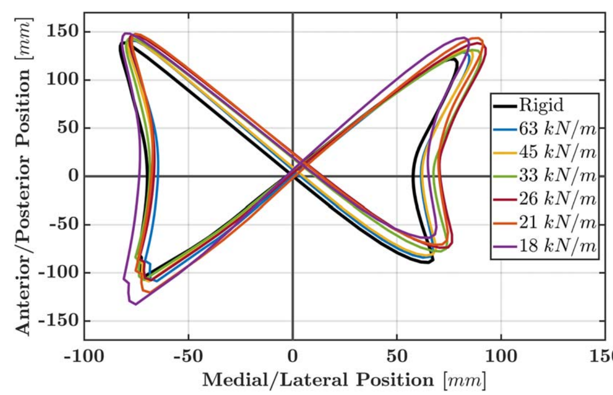

Fig. 11 Center of pressure path over a single gait cycle at multiple right-side unilateral stiffness levels with a 90 kg subject. The origin of [0, 0] is the subject's center of mass estimated by motion capture markers on the hips, projected on the walking plane. With this orientation of the figure, the subject is walking in the upward direction.

projected on the walking plane. The center of mass was estimated using four motion capture markers on the left and right, anterior and posterior superior iliac spine. In other words, if the center of pressure path is at [0, 0], the center of pressure is located directly below the center of mass.

The purpose of this brief experiment is not to prove the accuracy of the VST 2, as this has already been shown in Sec. 3.2, but is instead to demonstrate stiffness levels for the dynamic loading condition present in human gait. The new capabilities of the VST 2 are highlighted by showing the *vertical* deflection profile, the ground reaction force profile, as well as the total center of pressure path. Note that the total center of pressure path was not possible previously on VST 1 as there was only a force mat under the left belt, not both.

First, the deflection of a treadmill platform is displayed for different stiffness levels (see Fig. 9). The deflection of the platform follows the expected trend of lower stiffness level leading to more deflection. With a 90 kg subject, the platform has a maximum deflection of about 50 mm. The force applied to this platform in the vertical direction is also shown for each stiffness level (see Fig. 10). A similar trend is seen for the vertical ground reaction force. As the stiffness level decreases, more force is applied. Also, the shape of the curve changes from the standard "double peak" to close to a single peak.

Next, the total CoP ath is also distinguishable for different stiffness levels (see Fig. 11). For the rigid environment, the subject is centered left to right and front to back, as the path crosses close to [0,0]. As the stiffness levels become lower on the right side, there appears to be a trend of the subject shifting their weight to the right side. This trend can be seen by the path crossing to the right of the origin and by the path reaching farther in the positive x-direction. It would also appear that as the stiffness decreases, the left leg is riding the treadmill for longer, and the left hip is going into more extension near the toe off. This can be seen by the more negative y-values on the left lobe of the plot.

These brief results are quite preliminary, and the device will soon be adequately investigated with multiple subjects and an extensive experimental protocol. These results do, however, demonstrate a few of the capabilities of VST 2, most notably, those that are different from or not possible on VST 1. Besides the quantitative results discussed earlier, there has been excellent qualitative feedback while testing the device. Subjects find the VST 2 significantly more comfortable than the VST 1 due to the increased platform size, reduced noise, and reduced height.

4 Conclusions

This article presents the design and validation of the VST 2, which includes substantial and significant improvements compared to the previous version of the VST. First, the VST 2 generates vertical deflection instead of the angular deflection in the VST 1. Second, this device is a split-belt treadmill capable of independently altering the stiffness of both belts within a range of 13 kN/m to 1.5 MN/m. Also, the speed of the belts is independent, as each belt has a dedicated motor. Next, the VST 2 has a large walking surface that allows for comfortable walking or running. Last, this device is instrumented with high-spatial-resolution force mats underneath the treadmill belts that enable the collection of ground reaction forces and the foot center of pressure.

The VST 2 was evaluated through validation experiments. First, an experimental stiffness curve was found by applying a 70 kg mass to the treadmill platform with the carriage at multiple different positions. That allowed for a comparison between the theoretical and experimental stiffness curves. The discrepancy between these curves led to a remapping of the relationship between carriage position and stiffness, by fitting a nonlinear curve to the "usable" portion of the experimental data ($R^2 = 0.9998$). This new mapping was then validated through a step-response analysis, showing that the VST 2 can generate a desired stiffness with less than 1% error and less than a 2.2 kN/m standard deviation, proving high accuracy and repeatability. Moreover, preliminary experiments with human subjects showed that the VST 2 could accurately and robustly control the belt stiffness under dynamic loading while maximizing comfort. Most importantly, the preliminary human subjects experiments show that the developed platform allows for the collection and analysis of gait data that have not been possible by other devices, such as the center of pressure path, among others.

With high accuracy and precision, along with the additional upgrades and features, the VST 2 is a unique device with much research and commercial value. This device, with the options of bilateral stiffness and velocity control, will allow for more comprehensive research in the areas of biomechanics, robotics, rehabilitation, and motor control. This device will soon be used with affected populations (stroke and lower limb amputees) to test rehabilitation protocols and prosthetic controller design. Also, in the near future, the VST 2 will be used with legged robots to refine control strategies for many of the terrains they would experience in the real world.

Acknowledgment

We thank Noah Stiebritz for his contribution to the software development related to the VST 2 platform and Sydney Przywara for her contribution to the initial design of the VST 2.

Funding Data

- National Science Foundation (Grant Nos. 2020009, 2015786, 2025797, and 2018905).
- National Institutes of Health (Grant No. 1R01HD111071-01).
- Partially supported by the Onassis Foundation – Scholarship ID: F ZQ029-1/2020-2021.

Conflict of Interest

There are no conflicts of interest.

Data Availability Statement

No data, models, or code were generated or used for this paper.

References

[1] Kowalsky, D. B., Rebula, J. R., Ojeda, L. V., Adamczyk, P. G., and Kuo, A. D., 2021, "Human Walking in the Real World: Interactions Between Terrain Type, Gait Parameters, and Energy Expenditure," PLoS One, **16**(1), p. e0228682.
[2] Reisman, D. S., Block, H. J., and Bastian, A. J., 2005, "Interlimb Coordination During Locomotion: What Can Be Adapted and Stored?," J. Neurophysiol., **94**(4), pp. 2403–2415.
[3] Sousa, A. S. P., and Tavares, J. M. R. S., 2015, "Interlimb Coordination During Step-to-Step Transition and Gait Performance," J. Motor Behav., **47**(6), pp. 563–574.
[4] Skidmore, J., and Artemiadis, P., 2016, "Unilateral Walking Surface Stiffness Perturbations Evoke Brain Responses: Toward Bilaterally Informed Robot-Assisted Gait Rehabilitation," Proceedings - IEEE International Conference on Robotics and Automation, Stockholm, Sweden, May 16–21, IEEE, pp. 3698–3703.
[5] Chambers, V., and Artemiadis, P., 2023, "Using Robot-Assisted Stiffness Perturbations to Evoke Aftereffects Useful to Post-stroke Gait Rehabilitation," Front. Rob. AI, **9**, p. 1073746.
[6] Mesesan, G., Englsberger, J., Garofalo, G., Ott, C., and Albu-Schäffer, A., 2019, "Dynamic Walking on Compliant and Uneven Terrain Using DCM and Passivity-Based Whole-Body Control," 2019 IEEE-RAS 19th International Conference on Humanoid Robots (Humanoids), Toronto, Canada, Oct. 15–17, pp. 25–32.
[7] Hobbs, B., and Artemiadis, P., 2020, "A Review of Robot-Assisted Lower-Limb Stroke Therapy: Unexplored Paths and Future Directions in Gait Rehabilitation," Front. Neurorob., **14**, p. 19.
[8] Feigin, V. L., Brainin, M., Norrving, B., Martins, S., Sacco, R. L., Hacke, W., Fisher, M., Pandian, J., and Lindsay, P., 2022, "World Stroke Organization (WSO): Global Stroke Fact Sheet 2022," Int. J. Stroke, **17**(1), pp. 18–29.
[9] Duncan, P. W., Zorowitz, R., Bates, B., Choi, J. Y., Glasberg, J. J., Graham, G. D., Katz, R. C., Lamberty, K., and Reker, D., 2005, "Management of Adult Stroke Rehabilitation Care," Stroke, **36**(9), pp. e100–e143.
[10] Su, Y. R. S., Veeravagu, A., and Grant, G., 2016, "Neuroplasticity After Traumatic Brain Injury," *Translational Research in Traumatic Brain Injury*, D. Laskowitz and G. Grant, eds., CRC Press, Boca Raton, FL, pp. 163–178.
[11] Daly, J. J., and Ruff, R. L., 2007, "Construction of Efficacious Gait and Upper Limb Functional Interventions Based on Brain Plasticity Evidence and Model-Based Measures for Stroke Patients," Sci. World J., **7**, pp. 2031–2045.
[12] Sunderland, A., Tinson, D. J., Bradley, E. L., Fletcher, D., Langton Hewer, R., and Wade, D. T., 1992, "Enhanced Physical Therapy Improves Recovery of Arm Function After Stroke. A Randomised Controlled Trial," J. Neurol., Neurosur. Psych., **55**(7), p. 530 LP.
[13] Cavanagh, P. R., and Lafortune, M. A., 1980, "Ground Reaction Forces in Distance Running," J. Biomech., **13**(5), pp. 397–406.
[14] Hreljac, A., 2004, "Impact and Overuse Injuries in Runners.," Med. Sci. Spor. Exerc., **36**(5), pp. 845–849.
[15] Alnahdi, A. H., Zeni, J. A., and Snyder-Mackler, L., 2012, "Muscle Impairments in Patients With Knee Osteoarthritis," Sports Health, **4**(4), pp. 284–292.
[16] Tyler, T. F., Fukunaga, T., and Gellert, J., 2014, "Rehabilitation of Soft Tissue Injuries of the Hip and Pelvis," Int. J. Sports Phys. Therapy, **9**(6), p. 785.
[17] Jonathan, C., 2022, "Knee Rehab Exercises," https://www.verywellhealth.com/knee-rehab-exercises-2549750, Accessed August 14, 2024.
[18] Xie, K., Lyu, Y., Zhang, X., and Song, R., 2021, "How Compliance of Surfaces Affects Ankle Moment and Stiffness Regulation During Walking," Front. Bioeng. Biotechnol., **9**, pp. 1–10.
[19] Ferris, D. P., Liang, K., and Farley, C. T., 1999, "Runners Adjust Leg Stiffness for Their First Step on a New Running Surface," J. Biomech., **32**(8), pp. 787–794.
[20] Farley, C. T., Houdijk, H. H., Van Strien, C., and Louie, M., 1998, "Mechanism of Leg Stiffness Adjustment for Hopping on Surfaces of Different Stiffnesses," J. Appl. Physiol., **85**(3), pp. 1044–1055.
[21] Nalam, V., Bliss, C., Russell, J. B., Save, O., and Lee, H., 2022, "Understanding Modulation of Ankle Stiffness During Stance Phase of Walking on Different Ground Surfaces," IEEE Rob. Autom. Lett., **7**(4), pp. 9294–9301.

[22] Chang, M. D., Sejdić, E., Wright, V., and Chau, T., 2010, "Measures of Dynamic Stability: Detecting Differences Between Walking Overground and on a Compliant Surface," Human Move. Sci., **29**(6), pp. 977–986.
[23] Drolet, M., Yumbla, E. Q., Hobbs, B., and Artemiadis, P., 2020, "On the Effects of Visual Anticipation of Floor Compliance Changes on Human Gait: Towards Model-Based Robot-Assisted Rehabilitation," 2020 IEEE International Conference on Robotics and Automation (ICRA), Paris, France, May 31–Aug. 31, IEEE, Institute of Electrical and Electronics Engineers Inc, pp. 9072–9078.
[24] Angelidou, C., and Artemiadis, P., 2023, "On Predicting Transitions to Compliant Surfaces in Human Gait via Neural and Kinematic Signals," IEEE. Trans. Neural. Syst. Rehabil. Eng.,**31**, pp. 2214–2223.
[25] Hobbs, B., and Artemiadis, P., 2022, "A Systematic Method for Outlier Detection in Human Gait Data," 2022 International Conference on Rehabilitation Robotics (ICORR), Rotterdam, Netherlands, July 25–29, IEEE, pp. 1–6.
[26] Kerdok, A. E., Biewener, A. A., McMahon, T. A., Weyand, P. G., and Herr, H. M., 2002, "Energetics and Mechanics of Human Running on Surfaces of Different Stiffnesses," J. Appl. Physiol., **92**(2), pp. 469–478.
[27] Bellicoso, C. D., Bjelonic, M., Wellhausen, L., Holtmann, K., Günther, F., Tranzatto, M., Fankhauser, P., and Hutter, M., 2018, "Advances in Real-World Applications for Legged Robots," J. Field Rob., **35**(8), pp. 1311–1326.
[28] Karakasis, C., Poulakakis, I., and Artemiadis, P., 2022, "Robust Dynamic Walking for a 3d Dual-Slip Model Under One-Step Unilateral Stiffness Perturbations: Towards Bipedal Locomotion Over Compliant Terrain," 2022 30th Mediterranean Conference on Control and Automation (MED), Athens, Greece, June 28–July, pp. 969–975.
[29] Bosworth, W., Whitney, J., Kim, S., and Hogan, N., 2016, "Robot Locomotion on Hard and Soft Ground: Measuring Stability and Ground Properties In-Situ," Proceedings—IEEE International Conference on Robotics and Automation, Stockholm, Sweden, May 16–21,, Institute of Electrical and Electronics Engineers Inc., pp. 3582–3589.
[30] Fahmi, S., Focchi, M., Radulescu, A., Fink, G., Barasuol, V., and Semini, C., 2020, "Stance: Locomotion Adaptation Over Soft Terrain," IEEE Trans. Rob., **36**(2), pp. 443–457.
[31] Barkan, A., Skidmore, J., and Artemiadis, P., 2014, "Variable Stiffness Treadmill (VST): A Novel Tool for the Investigation of Gait," Proceedings—IEEE International Conference on Robotics and Automation, Hong Kong, China, May 31–June 7, Vol. 9, pp. 2838–2843.
[32] Skidmore, J., Barkan, A., and Artemiadis, P., 2015, "Variable Stiffness Treadmill (VST): System Development, Characterization, and Preliminary Experiments," IEEE/ASME Trans. Mechatron., **20**(4), pp. 1717–1724.
[33] Skidmore, J., and Artemiadis, P., 2015, "Leg Muscle Activation Evoked by Floor Stiffness Perturbations: A Novel Approach to Robot-Assisted Gait Rehabilitation," 2015 IEEE International Conference on Robotics and Automation (ICRA), Seattle, WA, May 26–30, pp. 6463–6468.
[34] Skidmore, J., and Artemiadis, P., 2016, "On the Effect of Walking Surface Stiffness on Inter-limb Coordination in Human Walking: Toward Bilaterally Informed Robotic Gait Rehabilitation," J. NeuroEng. Rehabil., **13**(1), p. 32.
[35] Skidmore, J., and Artemiadis, P., 2019, "A Comprehensive Analysis of Sensorimotor Mechanisms of Inter-Leg Coordination in Gait Using the Variable Stiffness Treadmill: Physiological Insights for Improved Robot-Assisted Gait Therapy," 2019 IEEE 16th International Conference on Rehabilitation Robotics (ICORR), Toronto, Canada, June 24–28, pp. 28–33.
[36] Skidmore, J., and Artemiadis, P., 2016, "Unilateral Floor Stiffness Perturbations Systematically Evoke Contralateral Leg Muscle Responses: A New Approach to Robot-Assisted Gait Therapy," IEEE. Trans. Neural. Syst. Rehabil. Eng., **24**(4), pp. 467–474.
[37] Chambers, V., and Artemiadis, P., 2022, "Repeated Robot-Assisted Unilateral Stiffness Perturbations Result in Significant Aftereffects Relevant to Post-Stroke Gait Rehabilitation," IEEE International Conference on Robotics and Automation (ICRA), Philadelphia, PA, May 23–27, IEEE, pp. 5426–5433.
[38] Hernandez, E., Warhmund, C., Lamoureux, K., Lee, E., Sanchez, I., Matthews, W., and Jafari, A., 2018, "A Novel Treadmill That Can Bilaterally Adjust the Vertical Surface Stiffness," IEEE/ASME Trans. Mechatron., **23**(5), pp. 2338–2346.
[39] MP, M., 1970, "Walking Patterns of Normal Woman," Arch. Phys. Med. Rehabil., **51**, pp. 637–650.
[40] Murray, M. P., Drought, A. B., and Kory, R. C., 1964, "Walking Patterns of Normal Men," JBJS, **46**(2), pp. 335– 360.
[41] Jafari, A., and Ebrahimi, N., 2021, "Chapter 7—TwAS: Treadmill With Adjustable Surface Stiffness," Soft Robotics in Rehabilitation, A. Jafari and N. Ebrahimi, eds., Academic Press, Cambridge, MA, pp. 199–240.
[42] Reisman, D. S., Wityk, R., Silver, K., and Bastian, A. J., 2007, "Locomotor Adaptation on a Split-Belt Treadmill Can Improve Walking Symmetry Post-stroke," Brain: A J. Neurol., **130**(Pt 7), pp. 1861–1872.
[43] Reisman, D. S., McLean, H., Keller, J., Danks, K. A., and Bastian, A. J., 2013, "Repeated Split-Belt Treadmill Training Improves Poststroke Step Length Asymmetry," Neurorehabil. Neural Repair, **27**(5), pp. 460–468.
[44] Huynh, K. V., Sarmento, C. H., Roemmich, R. T., Stegemöller, E. L., and Hass, C. J., 2014, "Comparing Aftereffects After Split-belt Treadmill Walking and Unilateral Stepping," Med. Sci. Sports. Exercise., **46**(7), pp. 1392–1399.
[45] Lee, Y.-J., and Liang, J. N., 2020, "Characterizing Intersection Variability of Butterfly Diagram in Post-stroke Gait Using Kernel Density Estimation," Gait Posture, **76**, pp. 157–161.
[46] Bosworth, W., Whitney, J., Kim, S., and Hogan, N., 2016, "Robot Locomotion on Hard and Soft Ground: Measuring Stability and Ground Properties In-Situ," 2016 IEEE International Conference on Robotics and Automation (ICRA), Stockholm, Sweden, May 16–21, pp. 3582–3589.
[47] Reisman, D. S., Wityk, R., Silver, K., and Bastian, A. J., 2009, "Split-Belt Treadmill Adaptation Transfers to Overground Walking in Persons Poststroke," Neurorehabil. Neural Repair, **23**(7), pp. 735–744.
[48] Miéville, C., Lauzière, S., Betschart, M., Nadeau, S., and Duclos, C., 2018, "More Symmetrical Gait After Split-Belt Treadmill Walking Does Not Modify Dynamic and Postural Balance in Individuals Post-stroke," J. Electromyogr. Kinesiol., **41**, pp. 41–49.
[49] Tsagarakis, N. G., Sardellitti, I., and Caldwell, D. G., 2011, "A New Variable Stiffness Actuator (CompAct-VSA): Design and Modelling," 2011 IEEE/RSJ International Conference on Intelligent Robots and Systems, San Francisco, CA, Sept. 25–30, IEEE, pp. 378–383.
[50] Zhou, X., Jun, S.-k., and Krovi, V., 2015, "A Cable Based Active Variable Stiffness Module With Decoupled Tension," J. Mech. Rob., **7**(1), p. 011005.
[51] Jafari, A., Tsagarakis, N. G., and Caldwell, D. G., 2011, "A Novel Intrinsically Energy Efficient Actuator With Adjustable Stiffness (AwAS)," IEEE/ASME Trans. Mechatron., **18**(1), pp. 355–365.
[52] Sun, J., Guo, Z., Sun, D., He, S., and Xiao, X., 2018, "Design, Modeling and Control of a Novel Compact, Energy-Efficient, and Rotational Serial Variable Stiffness Actuator (SVSA-II)," Mech. Mach. Theory., **130**, pp. 123–136.
[53] Sun, J., Guo, Z., Zhang, Y., Xiao, X., and Tan, J., 2018, "A Novel Design of Serial Variable Stiffness Actuator Based on an Archimedean Spiral Relocation Mechanism," IEEE/ASME Trans. Mechatron., **23**(5), pp. 2121–2131.